IEEE Access
Multidisciplinary | Rapid Review | Open Access Journal

Received 28 June 2023, accepted 31 July 2023, date of publication 14 August 2023, date of current version 21 August 2023.

Digital Object Identifier 10.1109/ACCESS.2023.3305253

RESEARCH ARTICLE

Minimization of Mutual Coupling Interferences Between Nearby Antenna Arrays to Retain Their Beam Steering Functionality

HSI-TSENG CHOU[1], (Fellow, IEEE), CHEN-YI CHANG[1], (Graduate Student Member, IEEE), AND DANAI TORRUNGRUENG[2], (Senior Member, IEEE)

[1]Graduate Institute of Communication Engineering, National Taiwan University, Taipei 10617, Taiwan
[2]Research Center of Innovation Digital and Electromagnetic Technology, Department of Teacher Training in Electrical Engineering, Faculty of Technical Education, King Mongkut's University of Technology North Bangkok, Bangkok 10800, Thailand

Corresponding author: Danai Torrungrueng (dtg@ieee.org)

This work was supported in part by the National Science and Technology Council, Taiwan; in part by the National Science, Research and Innovation Fund (NSRF); and in part by the King Mongkut's University of Technology North Bangkok under Contract KMUTNB-FF-66-46.

ABSTRACT This paper presents an effective excitation synthesis algorithm of phased arrays of antennas to optimize the radiation patterns under minimum mutual coupling/induction interferences between two nearby arrays. The optimization goal is to minimize the inter-array interferences in an attempt to retain their radiation beam characteristics. Furthermore, a cost function is defined to reduce the inter-array reaction and the excitation weighting deviations from the desired ones for directional beam radiations by embedding a coupling reduction factor (CRF). The resulting solutions are in a simple closed-form for easy implementation. Besides, the mutual coupling/induction mechanisms are effectively interpreted using the singular-value decomposition (SVD) method to create an eigenspace for signal representations and the complementary null space. Finally, theoretical and numerical full-wave simulation examples are presented to validate the proposed mutual coupling/induction suppression method.

INDEX TERMS Antenna array, array synthesis, beam-steering, electromagnetic interferences, pattern nulling, singular-value decomposition.

I. INTRODUCTION

Modern wireless communications and radar systems widely use phased arrays of antennas [1], [2], [3] to provide sufficient gains. Indeed, many applications employ several antenna systems to cover different angular sectors or separate transmitting and receiving antenna arrays, such as in radar systems [4], [5]. For example, various operators' base transceiver system (BTS) antennas in mobile communications may be co-sited to save space [6]. Aircraft or ships may install several antennas on their bodies to cover communications and radar detections in different directions [7]. These antenna arrays are placed very close to each other and result in large electromagnetic (EM) interferences [4], [5], [6], [7], [8], [9] through the mutual coupling/induction between them. These interferences are especially severe when the directional beams of a transmitting (TX) antenna array are steered toward the directions very close to the positions of neighborhood receiving (RX) antenna arrays which receive the illuminating EM fields to cause interferences. For example, in long-distance radar detection, the strength of echo signals may be weaker than the inter-array coupled power to cause misestimation.

Past works examining the mutual-coupling interferences focused on analysis based on EM numerical techniques [7], [10], [11], [12], [13]. The interference can be reduced by implementing hardware structures. Common approaches build EM bandgap (EBG) or EBG-like

The associate editor coordinating the review of this manuscript and approving it for publication was Claudio Curcio.

structures [5], [8], [9], [14], [15], [16] or defected ground planes [17] between the two antenna arrays. These approaches increase structural complexity and may better suppress surface waves when implemented on the same planar substrates or joint convex surfaces. They do not apply to the array cases where the two arrays have partial line-of-sight (LOS) visible contact or are not implemented on the same platforms. Also, fabrication discrepancies may degrade the isolation performance.

Most previous works considered a far-field scenario in terms of antenna radiation synthesis. It is intuitive to place these arrays in the sidelobe regions of other arrays' radiations to avoid main beam blockages in beam steering, as in the conventional anti-jamming design. Far-field sidelobe levels (SLLs) [4] are applied to TX and RX antenna array cases. Typical examples include Chebyshev [18], [19], [20], [21] or Taylor [19], [22] array distributions. These global SLL suppressions may result in over-synthesizing the radiation patterns to cause gain degradation because the arrays' physical areas occupy only a small angular portion. SLL suppression over the angular range of the RX antenna arrays is much desired to minimize the gain and beamwidth performance degradation.

Other approaches of far-field pattern synthesis for the TX antenna arrays produce a confined angular null-field range [23], [24], [25], [26], [27], [28], [29] covering the RX antennas. However, they are applicable only when the arrays are long separated to make good EM field propagation behaviors and resemble far-field patterns from TX and RX antenna arrays. In such scenarios, adaptive nulling techniques [30] can be employed, including the well-known Schelkunoff polynomial method [18], [19], broadening null techniques [31], [32], [33], and other similar methods based on the digital signal process (DSP) [4], [34], [35]. In particular, the works in [34] and [35] perform radiation nulling to avoid user interferences in mobile communications. Near-field nulling was employed in [36] to avoid radiation blockage, which results in low SLLs in an angular range.

These approaches have the advantage of synthesizing the TX and RX antenna arrays' radiation patterns in standing-alone procedures to simplify the computational complexity. They may, however, result in excessive gain drops and beam distortions when the TX and RX arrays are too close in their relative angular positions. They are also inapplicable when the EM near-field mutual coupling between TX and RX antenna arrays is strong because of their close positions. Besides, they cannot be applied to near-field radiation applications like bio-sensing systems. In these near-field mutual coupling cases, conventional far-field pattern nulling does not necessarily assure small EM coupling/induction in a near-zone due to their Fourier transform relationship [19]. Note that the net interference effects are primarily determined by the mutual reactions [37], [38], [39] between the two arrays at the excitation ports of beamform networks (BFNs) from the system point of view. Thus, proper excitation weightings of all antenna arrays contribute to end-to-end interference suppression. Therefore, the design goal should minimize the EM coupling/induction interferences while retaining the original beam characteristics.

This paper defines a cost function first incorporating the deviations of array excitations between the original ones of directional beam steering for radiation pattern synthesis [40], [41], [42] and the optimized ones. These deviations in the cost function shall be minimized to find the optimized excitation by reducing the beam distortion because the excitation deviations will cost gain drops. Afterward, the cost function incorporates the EM reactions between the TX and RX antenna arrays with a ratio by a complex coupling reduction factor (CRF). This CRF compromises its weighting between the reaction power and the excitation deviations. It is a varying parameter for minimizing cost function to manually control the suppression levels of inter-array reaction and gain drops. A proper tradeoff can be achieved by selecting an appropriate CRF value from observing the gain drop and reaction power variations for good antenna performance. This avoids solving sophisticated matrix equations in the minimization problems and provides a closed-form formulation. To interpret the suppression mechanism, the reaction matrices between the paired arrays are analyzed by the singular-value decomposition (SVD) method [39], [41], [42] to find the signal and null spaces of mutual coupling between the antenna arrays. The analysis results in closed-form solutions corresponding to the original excitations with a correction term of subtracting the projected weightings in the eigenspace spanning the physical coupling mechanisms. They can be applied to both near- and far-field radiation applications. The antenna arrays can also be in the others' near- or far-field region according to a reasonable arrangement and configuration.

The rest of the paper is organized in the following format. Section II summarizes the essential theoretical foundation of EM mutual coupling/induction between two antenna arrays. Then, the solutions to minimize the coupling interferences are developed by the SVD analysis. The extension to treat multiple array problems is presented in Section III. Demonstration examples are presented in Section IV to validate the feasibility. In addition, Section V illustrates the full-wave simulation validation. Finally, conclusive remarks and future phase studies are discussed in Section VI.

II. FORMULATION OF EM MUTUAL COUPLING INTERFERENCES BETWEEN TWO ANTENNA ARRAYS

A. APPLICATION SCENARIO AND DEFINING THE COST FUNCTION

Consider two paired nearby TX and RX antenna arrays of N and M elements, respectively, as illustrated in Fig. 1 We assume that the beamforming networks (BFNs) consist of RF power splitters/combiners to produce single port excitations. The RF devices in the BFNs consist of amplitude and phase controllers, including digital phase shifters (DPSs), power/low-noise amplifiers (PA/LNA), and attenuators for the system operations. Thus, the EM mutual coupling

interferences are justified by the net signal strengths at the output ports of the BFNs. Let the array excitations be $A_{1\times N} = [a_n(n = 1 \sim N)]$ and $B_{1\times M} = [b_m(m = 1 \sim M)]$ for TX and RX arrays, respectively. The reaction matrix of mutual coupling between the TX and RX arrays is represented by S_{TR} as [38], [39], [43], [44].

$$S_{TR} = [g_{nm}] = \begin{bmatrix} g_{11} & g_{12} & \cdots & g_{1(M-1)} & g_{1M} \\ g_{21} & g_{22} & \cdots & & g_{2M} \\ \vdots & \vdots & \ddots & & \vdots \\ g_{(N-1)1} & & \cdots & & g_{(N-1)M} \\ g_{N1} & g_{N2} & \cdots & g_{N(M-1)} & g_{NM} \end{bmatrix} \quad (1)$$

This reaction matrix is proportional to the scattering matrix [45], [46], [47] and mutual impedance matrix [46], [47] for two fixed arrays. Thus, They can be flexibly extracted from either full-wave simulations or measurements between antenna excitation ports without losing applicability because the constant ratios do not alter the results. The reaction matrix incorporates the effect of antenna radiation and allows the TX and RX arrays to use different antenna configurations or elemental antenna types. They are not limited to be planar, and can also be relatively conformal to a curved profile. The reaction power is related to the actual receiving power and is defined from the reaction theorem [39], [43] by [44]:

$$P_{rec} = \left| A_{1\times N} S_{TR} B^T_{1\times M} \right|^2 \quad (2)$$

where the superscript "T" denotes the matrix transpose. The target of optimization is to make $P_{rec} \rightarrow 0$. It is also noted that the reaction matrix, S_{TR}, also serves as a transformation matrix to transform the effects of the TX antenna array's excitation signals to the other RX antenna arrays and vice versa because the reaction matrix is reciprocal [39], [43], [44], [45], [46], [47], [48].

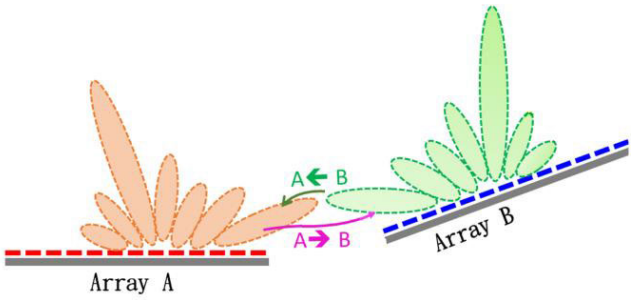

FIGURE 1. The radiation scenario of two antenna arrays is shown with mutual coupling interferences. Array A and B are in the TX and RX modes, respectively.

This work aims to minimize EM mutual coupling/induction interferences while retaining the original beam characteristics of TX and RX antenna arrays. Thus, a cost function is defined to correlate the EM coupling interferences with the deviation of excitation weightings by [28]

$$\Omega \equiv \left| \tilde{A}_{1\times N} - A_{1\times N} \right|^2 + \left| \tilde{B}_{1\times M} - B_{1\times M} \right|^2 + \alpha \left(\tilde{A}_{1\times N} S_{TR} \tilde{B}^T_{1\times M} \right) + \alpha^* \left(\tilde{A}_{1\times N} S_{TR} \tilde{B}^T_{1\times M} \right)^* \quad (3a)$$

where $A_{1\times N}$ and $B_{1\times M}$ are the excitation coefficients of the original beams while $\tilde{A}_{1\times N}$ and $\tilde{B}_{1\times M}$ are the varying ones for optimization to minimize the cost function. In (3a), the complex CRF, α, is introduced to compromise the weight between P_{rec} and the excitation coefficients' deviations. The solution to minimizing (3a) is identical to the case by directly incorporating the reaction power in (2) into the cost function by selecting

$$\alpha = \beta \left(\tilde{A}_{1\times N} S_{TR} \tilde{B}^T_{1\times M} \right)^* \quad (3b)$$

where β is a positive constant. The CRF is retained as a free variable in this paper to produce closed-form solutions.

Equation (3a) is minimized by solving the zero derivatives of (3a) with respect to $\tilde{A}_{1\times N}$ and $\tilde{B}_{1\times M}$. It can be expressed as

$$\begin{cases} \left(\tilde{A}_{1\times N} - A_{1\times N} \right) + \alpha^* \left(\tilde{B}^*_{1\times M} S^H_{TR} \right) = 0 \\ \left(\tilde{B}_{1\times M} - B_{1\times M} \right) + \alpha^* \left(\tilde{A}^*_{1\times N} S^*_{TR} \right) = 0 \end{cases} \quad (4)$$

where the superscript "H" is the matrix Hermitian, which has the following relationship after canceling the second terms of the two equations:

$$\left(\tilde{A}_{1\times N} - A_{1\times N} \right) \tilde{A}^H_{1\times N} = \left(\tilde{B}_{1\times M} - B_{1\times M} \right) \tilde{B}^H_{1\times M} \quad (5)$$

Note that if (3b) is incorporated into (4), it is challenging to find closed-form solutions. Freely varying of α is beneficial to solve (4) to give the following closed-form solutions:

$$\tilde{A}_{1\times N} = \left(A_{1\times N} - \alpha^* \left(S_{TR} B^T_{1\times M} \right)^H \right) \left(I_{N\times N} - |\alpha|^2 S_{TR} S^H_{TR} \right)^{-1} \quad (6)$$

and

$$\tilde{B}_{1\times M} = \left(B_{1\times M} - \alpha^* A^*_{1\times N} S^*_{TR} \right) \left(I_{M\times M} - |\alpha|^2 S^T_{TR} S^*_{TR} \right)^{-1} \quad (7)$$

The optimized excitations consist of two terms in (6) and (7). The terms associated with α are related to the TX radiations causing strong mutual couplings to the RX antenna array, which are related to the excitations of the influencing antennas and the reaction matrix. One plots the curves of normalized reaction power in (2) with respect to α and finds the desired values to minimize the normalized reaction power, thus minimizing mutual coupling effects.

B. MECHANISMS OF MUTUAL COUPLING SUPPRESSION BY SINGULAR-VALUE DECOMPOSITION

The solutions of (6) and (7) involve an inverse matrix which is referred to as the coupling suppression matrix (CSM). Indeed, S_{TR} defines the EM mutual coupling space. The null space is

complementary to minimize the mutual coupling. Thus, (6) and (7) represent the projections of $A_{1\times N}$ and $B_{1\times M}$ into the null space of S_{TR}. Thus, one obtains the eigenspace space of S_{TR} by performing SVD on it: [39], [41]

$$S_{TR}|_{N\times M} = U_{N\times N}\Lambda_{N\times M}(V_{M\times M})^H \tag{8}$$

where $U_{N\times N}$ and $V_{M\times M}$ are unitary matrices of eigenvectors, and $\Lambda_{N\times M}$ is a diagonal matrix of singular-values, λ_i, of S_{TR}. It is noted that there exist only Q non-zero positive singular-values, λ_i, arranged in a non-ascending order, where $Q = \min(N, M)$. For simplification, one lets $N \geq M$ to make $Q = M$. The case of $M \geq N$ can be performed similarly. One first expresses $U_{N\times N}$ and $\Lambda_{N\times M}$ in the following format:

$$U_{N\times N} = [U^{(1)}_{N\times M}\, U^{(2)}_{N\times(N-M)}] \tag{9}$$

and

$$\Lambda_{N\times M} = \begin{bmatrix} \Lambda^{(1)}_{M\times M} \\ O_{(N-M)\times M} \end{bmatrix} \tag{10}$$

where $\Lambda^{(1)}_{M\times M}$ is a diagonal matrix formed by the non-zero singular-values, while $O_{(N-M)\times M}$ is a zero matrix. In (9), $U^{(1)}_{N\times M}$ and $U^{(2)}_{N\times(N-M)}$ are associated with $\Lambda^{(1)}_{M\times M}$ and $O_{(N-M)\times M}$, respectively, identified as the signal and null spaces of S_{TR}, respectively. It can be shown that

$$\begin{cases} \left(I_{N\times N} - |\alpha|^2 S_{TR} S^H_{TR}\right) = U_{N\times N}\Lambda^{(A)}_{N\times N}U^H_{N\times N} \\ \left(I_{M\times M} - |\alpha|^2 S^T_{TR} S^*_{TR}\right) = V^*_{M\times M}\Lambda^{(B)}_{M\times M}\left(V^*_{M\times M}\right)^H \end{cases} \tag{11}$$

where

$$\Lambda^{(A)}_{N\times N} = \begin{bmatrix} \Lambda^{(B)}_{M\times M} & O_{M\times(N-M)} \\ O_{(N-M)\times M} & I_{(N-M)\times(N-M)} \end{bmatrix} \tag{12}$$

with

$$\Lambda^{(B)}_{M\times M} = \begin{bmatrix} 1-|\alpha|^2\lambda_1^2 & 0 & \cdots & 0 \\ 0 & 1-|\alpha|^2\lambda_2^2 & 0 & \vdots \\ \vdots & 0 & \ddots & 0 \\ 0 & \cdots & 0 & 1-|\alpha|^2\lambda_M^2 \end{bmatrix} \tag{13}$$

Note that both (12) and (13) are diagonal matrices whose inverse can be obtained in closed-form solutions. The CSMs in (11) represent the resulting contributions after removing the projecting in the eigenspace of S_{TR}. Also, (13) is a unit matrix after subtracting the square of the singular values of αS_{TR}. Fig. 2 shows the primary mechanism to format the net excitations by two mutual coupling terms and one without mutual coupling. One can see the coupling mechanisms between the two antenna arrays through the reaction theorem.

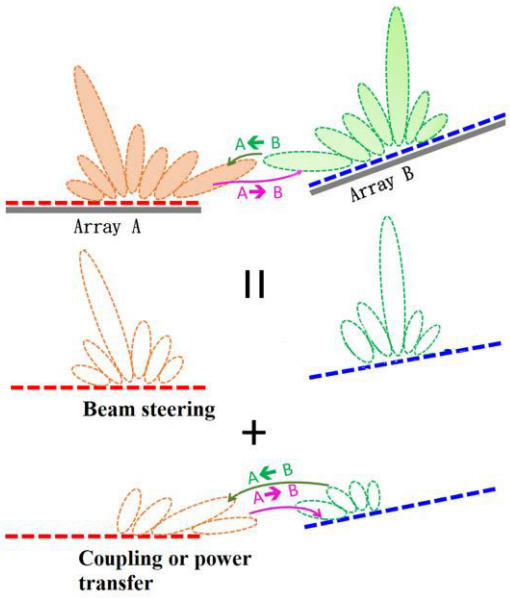

FIGURE 2. The excitations of antenna arrays are decomposed into two components for directional beam steering and mutual coupling, respectively.

The solutions in (6) and (7) can be further simplified in the eigenspaces of $U_{N\times N}$ and $(V_{M\times M})*$ by

$$\begin{cases} \tilde{A}^{(e)}_{1\times N} = \tilde{A}_{1\times N}U_{N\times N} \\ A^{(e)}_{1\times N} = A_{1\times N}U_{N\times N} \end{cases} \tag{14}$$

$$\begin{cases} \tilde{B}^{(e)}_{1\times M} = \tilde{B}_{1\times M}V^*_{M\times M} \\ B^{(e)}_{1\times M} = B_{1\times M}V^*_{M\times M} \end{cases} \tag{15}$$

where the superscript "(e)" implies the expression of excitations in the eigenspaces. The solutions in (6) and (7) become

$$\tilde{A}^{(e)}_{1\times N} = \left(\Lambda^{(A)}_{N\times N}\right)^{-1}\left(A^{(e)}_{1\times N} - \alpha^*(B^{(e)}_{1\times M})^*(\Lambda_{N\times M})^T\right) \tag{16}$$

and

$$\tilde{B}^{(e)}_{1\times M} = \left(\Lambda^{(B)}_{M\times M}\right)^{-1}\left(B^{(e)}_{1\times M} - \alpha^*(A^{(e)}_{1\times N})^*\Lambda_{N\times M}\right) \tag{17}$$

The $(B^{(e)}_{1\times M})^*(\Lambda_{N\times M})^T$ and $(A^{(e)}_{1\times N})^*\Lambda_{N\times M}$, in (16) and (17) represent transforming one array's excitations into a component of the other array's excitations. The behaviors of these components are analogous to exciting an RX array for maximum power transfer from the TX array by conjugate matching [39], [44], [49], except now the maximum power transfer is referred to as the maximum mutual coupling interferences in this work. The radiation decomposition in Fig. 2 can interpret the mechanism, where the original problem is decomposed into two issues of beam radiations and mutual coupling. These two transformed excitation components are related to the mutual-coupling transfer in the bottom scenario in Fig. 2. They should be subtracted from the original excitations to reduce the reaction power between the TX and RX

antenna arrays, as exhibited by the minus sign in (16) and (17). On the other hand, the middle plot in Fig. 2 involves creating low SLLs by the CSMs, as discussed in (11). The subtraction is desirable not to affect the main beam, as in the middle scenario of Fig. 2.

The computation of $(B^{(e)}_{1\times M})^*(\Lambda_{N\times M})^T$ in (16) reduced to

$$(B^{(e)}_{1\times M})^*(\Lambda_{N\times M})^T = \left[(B^{(e)}_{1\times M})^*(\Lambda^{(1)}_{M\times M})^T \; O_{1\times(N-M)}\right] \tag{18}$$

The terms of $\left(\Lambda^{(A)}_{N\times N}\right)^{-1}$ and $\left(\Lambda^{(B)}_{M\times M}\right)^{-1}$ are the normalization matrices to find the ratios between $A^{(e)}_{1\times N}$ and $B^{(e)}_{1\times M}$.

C. REDUCTION TO THE SPECIAL CASE OF FAR-FIELD ANTENNA ARRAYS

When both TX and RX antenna array elements are in the far zone of each other, the forming elements of the reaction matrix are related to their far-field radiation. The reaction between two paired antenna elements of unit excitation follows Friis' propagation equation. The element can be expressed in the following form: [37], [38]

$$g_{nm} \approx \frac{1}{Z_0}\bar{E}^T_n(\bar{R}_{nm})\cdot\bar{F}^R(\hat{R}_{nm}) \tag{19}$$

where the radiations of the TX and RX antenna elements are assumed to be in the following standard format:

$$\bar{E}^{T,R}_{n,m}(\bar{R}^{T,R}_{n,m}) = \frac{jke^{-jkR^{T,R}_{n,m}}}{4\pi R^{T,R}_{n,m}}\bar{F}^{T,R}(\hat{R}^{T,R}_{n,m}) \tag{20}$$

In (19) and (20), k is the wavenumber, R_{nm} is the distance between the TX and RX antennas, and Z_0 is the impedance of free space. In the far-field case, the operation of $A_{1\times N}S_{TR}$ can be simplified by

$$\begin{aligned} A_{1\times N}S_{TR} &= \frac{1}{2Z_0}\left(\sum_{n=1}^{N} a_n\bar{E}^T_n(\bar{R}_{nm})\right) \\ &= \frac{1}{2Z_0}\frac{jke^{-jkR_m}}{4\pi R_m}\bar{F}^T(\hat{R}_m)\left(\sum_{n=1}^{N} a_n e^{jk\left(\hat{R}_m\bullet\bar{r}'_{nm}\right)}\right) \end{aligned} \tag{21}$$

which is the far-field radiation from the TX antennas. The TX and RX arrays become a point-to-point interaction, resulting in a rank of one. The interference suppression reduces to nullifying TX antenna radiation patterns in the RX antenna directions.

III. GENERALIZATION TO THE MULTIPLE ARRAY SCENARIO

The proposed technique is generalized to treat multiple antenna arrays. One assumes $P(P \geq 2)$ nearby antenna arrays, where the p^{th} array has N_p antenna elements excited by $A_{p,1\times N_p}$. The reaction matrix between the p^{th} and q^{th} arrays is denoted by S_{pq}, where the mutual coupling power-related term is represented by $P_{pq} = |A_{p,1\times N_p}S_{pq}A^T_{q,1\times N_q}|^2$.

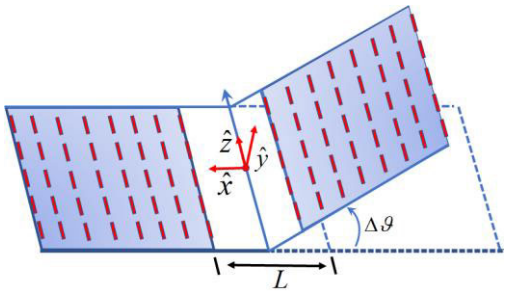

FIGURE 3. Configuration of two array systems to examine the mutual coupling effects and minimize the interferences.

The cost function is generalized from the format in (3a) by

$$\begin{aligned} \Omega \equiv \sum_{p=1}^{P}\left|\tilde{A}_{p,1\times N} - A_{p,1\times N}\right|^2 + \alpha\bigcup_2^P\left(\tilde{A}_{p,1\times N_p}S_{pq}\tilde{A}^T_{q,1\times N_q}\right) \\ + \alpha^*\bigcup_2^P\left(\tilde{A}_{p,1\times N_p}S_{pq}\tilde{A}^T_{q,1\times N_q}\right)^* \end{aligned} \tag{22}$$

where the notation "$\cup_2^P$" indicates the union of every two paired arrays' reaction or mutual coupling. When P=2, (22) reduces to (3a). The solution to minimizing the cost function in (22) is given by

$$\left(\tilde{A}_{p,1\times N_p} - A_{p,1\times N_p}\right) + \alpha^*\sum_{q=1,q\neq p}^{P}\left(\tilde{A}^*_{q,1\times N_q}S^*_{qp}\right) = 0;\ \forall p \tag{23}$$

The solution can be obtained by first expressing (23) in matrix equations and solving it by a matrix inverse.

IV. DEMONSTRATION EXAMPLES

A. NUMERICAL EXAMPLES BASED ON THEORETICAL MODELS OF ELEMENTAL ANTENNA RADIATION PATTERNS

Numerical examples of two-array cases, as illustrated in Fig. 3, are presented to validate the proposed method. The antenna arrays consist of 8 × 8 and 6 × 6 small dipoles for TX and RX arrays, respectively, which operates at the first fundamental mode to have a closed-form formulation of radiation. The periods are $\lambda/2$ for both arrays. These two arrays are first placed laterally side-by-side on the same plane, where the RX array is then bent to form an angle of $\Delta\vartheta$. Finally, the separation between the two adjacent edges of these two arrays is selected by $L = 10\lambda$. The dipole antenna arrays are intentionally considered to demonstrate the unique effectiveness of the proposed works because they have intense radiations along the cross-section directions to cause strong mutual couplings between the two arrays.

The inter-element mutual couplings on the same array are first put aside to focus on the synthesis of inter-array mutual coupling suppression for the optimal excitation weightings. They are then taken into account to find the actual terminal excitations. It is performed by multiplying the synthesized excitation weightings with the mutual impedance matrix of the same array, as exhibited in the conventional moment

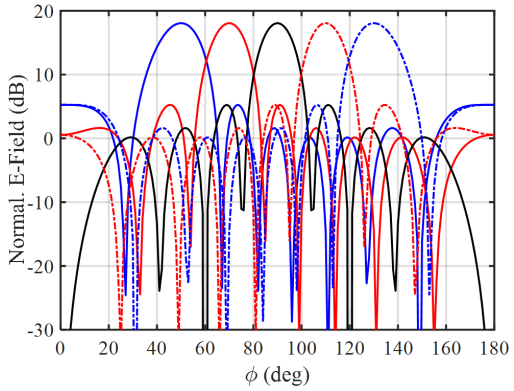

FIGURE 4. Radiation patterns from the TX antenna array excited by uniform amplitudes and linear phase progressions to radiate directional beams.

method [19], [50], [51] and embedded element pattern (EEP) techniques [52], [53], to find the actual excitations at the end-terminals. This will not alter the optimum radiation characteristics obtained by the proposed synthesis technique as this is an inverse pattern synthesis. The dipoles' electrical fields are given by the theoretical formula [19], [54]:

$$\bar{E}(\bar{r}) \simeq \bar{F}(\theta,\phi)\frac{jke^{-jkr}}{4\pi r}; \bar{F}(\theta,\phi) = (Z_0 I_0 \ell \sin\theta)\,\hat{\theta} \qquad (24)$$

where $I_0 = 1$, (r,θ,ϕ) is the representation of $\bar{r}$ in the spherical coordinate system, and ℓ is the dipole's size.

Figure 4 first shows the multi-beam radiation patterns of the TX antenna array at 38 GHz on the plane containing the centers of these two arrays when the array stands alone. Note that the RX array has similar patterns, which are thus omitted for brevity. In these cases, the TX array is steered with uniform amplitude and linear phase excitations to radiate main beams in the $\phi = 50^o$, 70^o, 90^o, 110^o and 130^o directions, respectively, where the constant terms in (24) are selected by a unit value to have a maximum field strength by a unit value at $\theta = 90^o$. The array factors are computed by the normalized excitation weightings to have a unit value of 0 dB power excitations. These patterns serve as the references to compare the results after the proposed method's optimization. In these cases, it is observed that the sidelobes are roughly -13.4 dB, as expected in theory, due to omnidirectional radiation patterns of dipoles.

To examine the reduction of mutual coupling interferences by the proposed technique, one selects $\Delta\vartheta = 15^o$ in Fig. 3, where the results are compared to the conventional directional nulling method by creating nulling field in the vicinity of $\phi = 165^o$ for the TX antenna array and $\phi = 15^o$ region for the RX antenna array. The reaction power in (2) is found for comparison, where the excitation weightings are normalized to unit power.

One first examines the effects of the complex CRF, α, on the reaction power and antenna radiation gains. One considers the case of boresight radiation in Fig. 4, where α is varied in the real axis to examine the behaviors. The

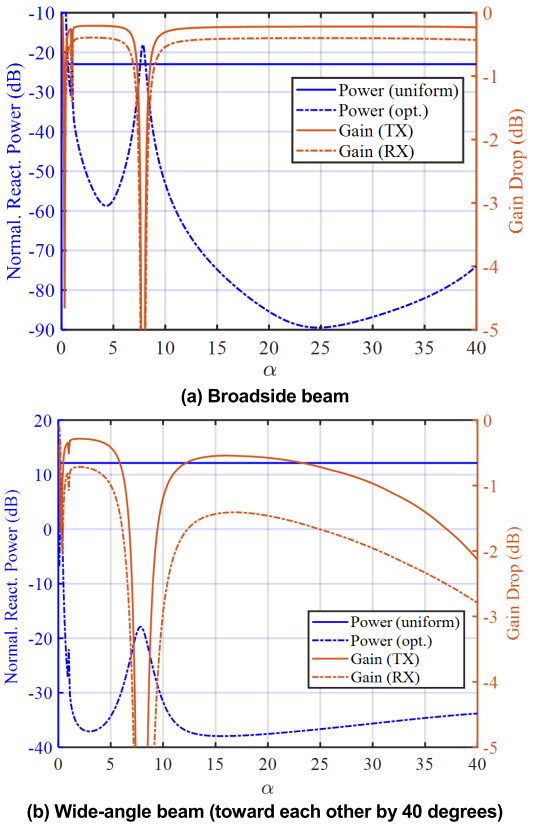

FIGURE 5. Comparisons of the normalized reaction powers and gain drops. The reaction powers are compared between the uniform excitations and the optimized excitations. The gain drops are for the TX and RX antenna arrays compared to the cases of uniform excitations.

normalized reaction power and the gain drops of the TX and RX antenna arrays are shown in Fig. 5(a). The normalized reaction powers obtained by the uniform and optimized excitations are compared. It is seen that the CRF significantly affects the reaction powers. When the reaction power is maximum, the gain drops are also large because most power propagates to the RX antenna array. The minimum value appears at $\alpha = 25$. At this value, the gain drops are also minimum for both TX and RX antenna arrays. This value will be used to compute the radiation patterns for comparison in Fig. 6(a). It is observed that the gain drop for the TX antenna array is less than 0.2 dB, which is less than 0.4 dB for the RX antenna array. Besides, the wide-angle sidelobes are significantly reduced, which exhibits null-like patterns. It is noted that the RX array is in the vicinity of $\phi = 165^o$ in the TX array's radiation, while the TX array is in the vicinity of $\phi = 15^o$ in the RX array's radiation. In these two regions, the radiations have very small field strengths to suppress the mutual coupling interferences. It is seen from Fig. 5 (a), the normalized reaction power reduces from -22.5 dB to -90 dB, i.e., 67.5 dB reductions.

One next considers a case of beam steering, where the beams of TX and RX antenna arrays are steered toward each other by 40 degrees to increase the mutual coupling. In other

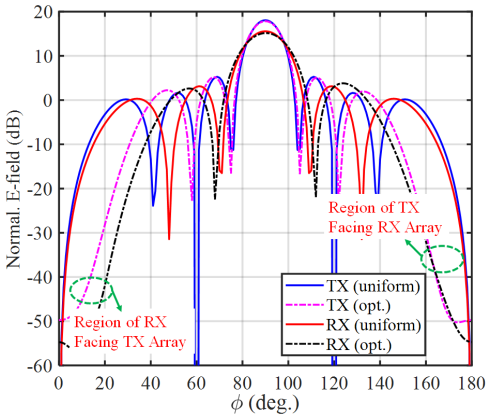

(a) Broadside beam

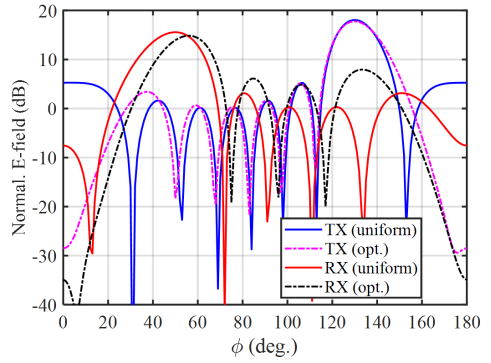

(b) Scan by 40° with a small RX array

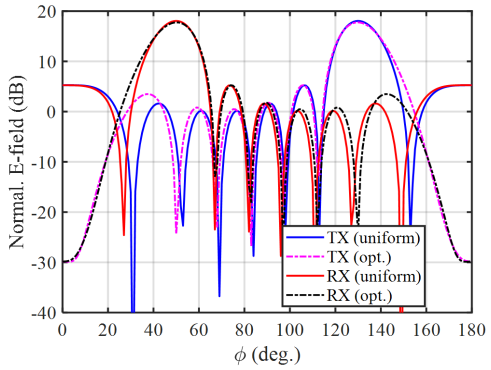

(c) Scan by 40° with a large RX array

FIGURE 6. Examinations of TX and RX antenna radiation patterns to study the effectiveness of the proposed suppression technique. In (b) and (c), the beams are scanned toward each other to increase the mutual coupling interferences.

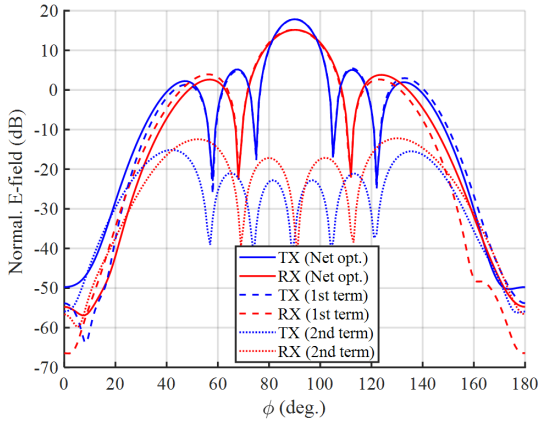

(a) Decomposed components in (5) and (6) with CSM

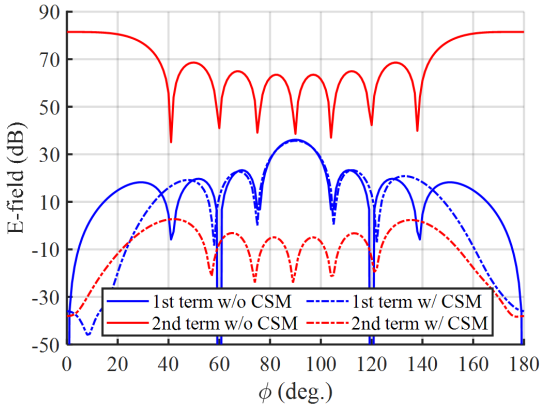

(b) Decomposed components in (5) for TX

FIGURE 7. Examinations of mutual coupling suppression mechanisms for each term in the solution format in (5) and (6) to show the effectiveness of the CSM.

words, the TX antenna beam is steered to 130°, while the RX antenna beam is steered to 50°. This wide-angle beam scan results in considerable mutual coupling interference between the two arrays, as shown by the normalized reaction power in Fig. 5(b), which can be as large as 12.5 dB. The proposed method is applied to reduce the reaction power by varying the CRF, α, where the results are shown in Fig. 5(b). Again, for reasonable values of α, the normalized reaction power reduction is more than 40 dB. Considering the minimum gain drops, the best value of α is roughly equal to 2, where the gain drops are approximately 0.3 and 0.7 dB for the TX and RX arrays. The resulting radiation patterns are shown in Fig. 6(b).

For the TX array, the main beam retains a good beam shape. The gain drops slightly to suppress the mutual coupling interferences at wide angles, which are more prominent on the right-hand side (RHS).

Similar behavior also appears to the RX antenna array's radiation pattern. However, a beam squint has been observed, which is caused by the small size of the antenna array and can be observed from the comparison of radiation patterns to the uniform excitation in Fig. 6(b). To verify this behavior, we increase the RX array's antenna elements to 8×8, and select $\alpha = 0.5$, resulting in the radiation patterns in Fig. 6(c). The normalized reaction powers are 27.7 dB and -34 dB for the uniform and optimized cases. The gain drops are roughly -0.28 dB.

One now examines the suppression mechanisms by considering the decomposed excitations by optimization in (5) and (6). As pointed out in Section II, the second terms associated with the α parameter excite the radiation to cause the mutual coupling interferences. Fig. 7(a) shows the contributions from each term in (5) and (6) for the TX and RX antenna arrays, respectively. It is seen that the second term associated with $\alpha*$ does not have significant contributions. This is because the patterns have low SLLs in the desired range of mutual

TABLE 1. Comparisons of reaction power between the TX and RX arrays by optimizing both arrays' excitations are shown (unit: dB).

Beam (deg)		50	70	90	110	130
W/o Opt	Abs. Val.	27.78	18.35	-19.97	19.64	27.73
Nulling	Abs. Val.	-25.56	-39.12	-62.58	-33.53	-19.55
	Reduction	53.34	57.47	42.61	53.17	47.28
This paper	CRF (α)	0.7	0.9	18.9	0.9	0.7
	Abs. Val.	-70.53	-71.37	-111	-82.6	-57
	Reduction	98.31	89.72	91.03	102.24	84.73

TABLE 2. Comparisons of gain drops between the TX and RX arrays by optimizing both arrays' excitations (unit: dB).

Beam (deg)		50	70	90	110	130
W/o Opt	Abs. Val.	18.06	18.06	18.06	18.06	18.06
Nulling	Abs. Val.	17	17.73	17.86	17.86	17
	Reduction	1.06	0.33	0.2	0.2	1.06
This paper	CRF (α)	0.7	0.9	18.9	0.9	0.7
	Abs. Val.	17.66	17.9	17.84	17.8	17.78
	Reduction	0.4	0.16	0.22	0.26	0.28

coupling suppression to provide a correction. However, the first term's contributions are close to the optimized ones for TX and RX antenna arrays.

Thus, one considers the effect of the CSMs in (5) and (6). Fig. 7(b) examines the two terms' effects in the radiation patterns for the TX antenna array. In this case, the excitation weightings are not normalized to explore the impact of the CSM. Again, the first term in (5) results in most of the desired patterns. The CSM tends to suppress the wide-angle sidelobes for mutual coupling suppression. Similar behaviors also appear in the second term of (5) to suppress the wide-angle sidelobes.

B. COMPARISON TO THE CONVENTIONAL PATTERN NULLING TECHNIQUE

One following compares the results to the conventional far-field nulling techniques [28] applied to the above-discussed cases. The nulling range is set by 0.02 in the $u = \sin\theta\cos\phi$ dimension to mutually accommodate the TX and RX arrays. The normalized reaction powers and radiation patterns are examined. Due to the symmetric orientation between the TX and RX antenna arrays, the beam steering is performed in the following 5 cases. For the TX beam steering to the 50°, 70°, and 90°, the RX's beams are steered to the same directions in their local coordinate systems.

On the other hand, for the TX beam steering to 90°, 110°, and 130° directions, the RX beams are steered to the opposite directions by 90°, 70°, and 50°, respectively, to increase the mutual coupling effects. Table 1 shows comparisons of reaction powers, while Table 2 shows the resulting gain drop comparisons. The CRFs, α, are selected to minimize the gain drops and reaction powers based on the procedure in Fig. 5. In all cases, the RX array consists of 8×8 elements.

It is first seen from Table 1 that the beam steering may alter the reaction power or mutual coupling interferences, especially when the main beams are close to the RX array

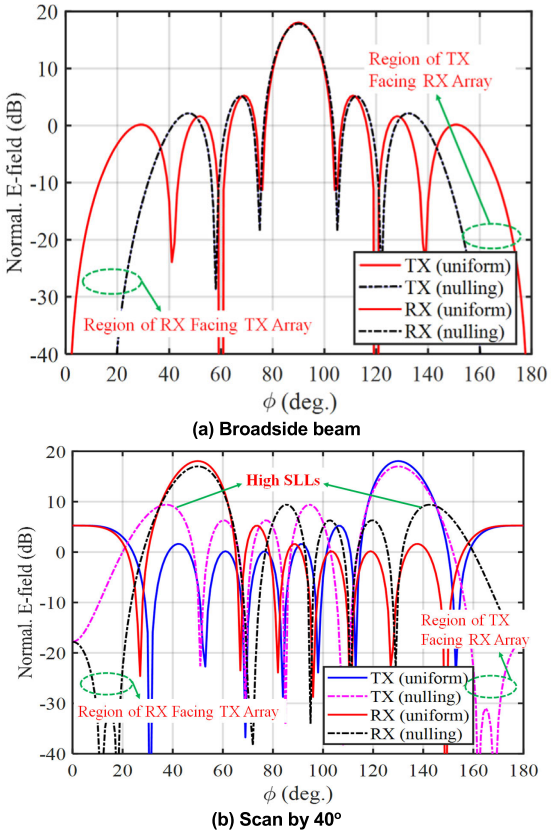

FIGURE 8. TX and RX antenna radiation patterns by nulling techniques compared with the proposed suppression technique. In (b), the beams are scanned toward each other to increase the mutual coupling interferences.

regions. After the optimization, the reductions can be larger than 60 dB by the proposed technique. On the other hand, the reductions by the pattern nulling technique on the reaction powers and gain drops are also shown in Tables 1 and 2. It is seen that in the broadside radiation, the nulling method to suppress mutual coupling also provides good performance. The gain drop is the same as the proposed technique. The reaction power is minimal by -62 dB in Table 1, or a 42.61 dB reduction. However, the proposed method reduces the reaction power to -95.93 dB, or a 75 dB reduction. It is better than the nulling technique by 33.3 dB. It is noted that when the beam is steered to wide angles, the performance of nulling approach becomes worse resulting in high gain drops. For example, when the beams of TX and RX arrays are steered by 40 degrees toward each other, i.e., in the case of TX beam steering to 130° in Tables 1 and 2, the gain drops increase to 1.06 dB, or 20% power loss. In this case, the reaction power is -19 dB, or 47.28 dB reduction, larger than the proposed technique by 15.3 dB.

The radiation patterns are shown in Fig. 8 (a) and (b) for the cases of TX beam steering to 90° and 130°, respectively. In the broadside beam case, the radiation patterns in Fig. 8(a) are similar to that of the proposed techniques. However, when the TX and RX beams are steered to 130° and 50°, the radiation patterns worsen, where the gain drop

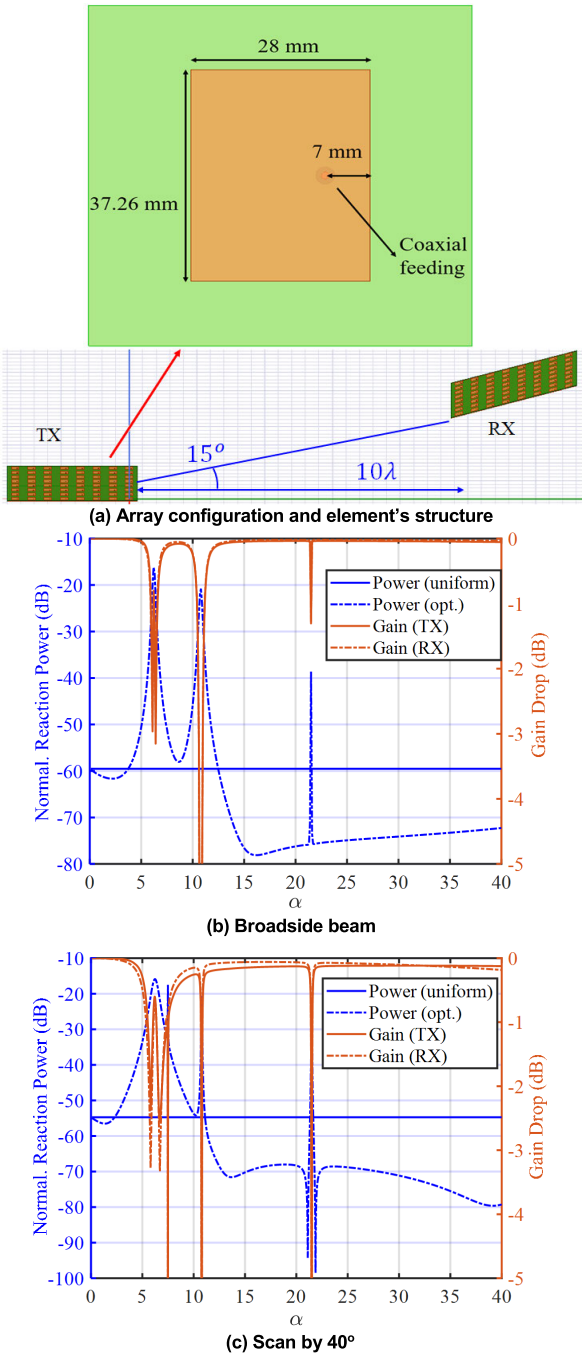

FIGURE 9. The array configuration between the TX and RX arrays and the element's structure in (a) are shown. The resulting reaction powers and gain drops for the broadside, and 40o beam scan are shown in (b) and (c), respectively. The CRF, α, is varied along $\varphi = 0.9\pi$ and 0.31π directions in its complex domain.

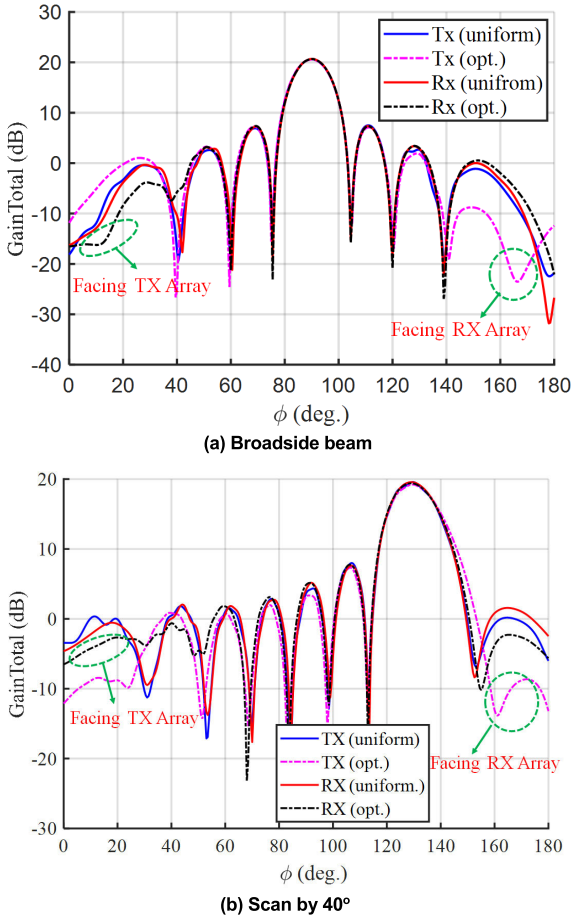

FIGURE 10. HFSS full-wave simulated radiation patterns of the resulting excitations by the proposed suppression technique. The patterns by uniform excitations are also shown for comparison.

is more than 1 dB. In these cases, the suppression regions are very close to the main beams in the first sidelobe regions. The SLLs also increase to -7.4 dB, producing grating lobe problems. The proposed technique performs better as it does not incur the SLL increase, as shown in Fig. 6(c). In most regions, the sidelobes remain reasonably unchanged from the original patterns. Thus, they demonstrate the superiority of the proposed method.

V. FULL-WAVE SIMULATION VALIDATION

Full-wave simulations by HFSS [55] on a realistic two-array configuration are presented to validate the proposed technique. The TX and RX arrays in the mutual coupling scenario have an identical configuration formed by 8×8 microstrip patch antennas at 2.5GHz. Fig. 9(a) shows the antenna element's configuration, with the dimensions labeled. The antennas are implemented on an FR4 dielectric substrate ($\varepsilon_r = 4.4 \tan\delta = 0.02$ and 1.6mm in thickness) for a lost cost. The periods are $\lambda/2$ in both the x and z dimensions for both arrays. Again, the tilted angle of the RX array in Fig. 3 is $\Delta\vartheta = 15^o$ for consistency with the studies in Sec. III, where the separation between the adjacent columns' centers of the two arrays is 10λ. In these cases, the mutual coupling between antenna elements inside the TX and RX antenna arrays is also incorporated to account for the actual mutual coupling interferences between the two arrays.

Following the same procedure in Section IV, one first finds the transmission S-matrix from the HFSS full-wave

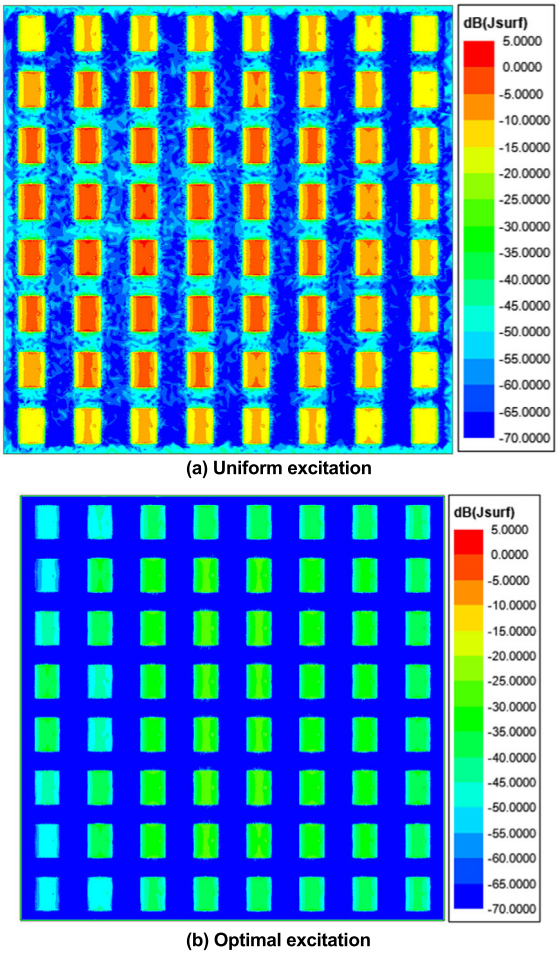

FIGURE 11. Comparison of the near-field equivalent current distributions on the RX array surface when the TX antenna array is excited by the uniform and the optimized excitations.

analysis between the TX and RX arrays. The process to obtain Fig. 5(a) and (b) is afterward performed, where the corresponding results are shown in Fig. 9 (b) and (c), respectively. In these cases, the beams of the two antenna arrays point to the broadside $\phi = 90^o$ and 130^o directions in their local coordinate systems.

The complex CRF, α, is varied along $\varphi = 0.9\pi$ and 0.31π directions in its complex domain to search for the minimum reaction powers. The variations of normalized reaction powers and gain drops in Fig. 9(b) and (c) show that $\alpha = 16.2$ and 21.87, respectively, give the best performances in terms of reaction powers and gain drops. After optimizing these beam steering cases, the normalized reaction powers are -79 and -99 dB, representing 19 and 43 dB reductions, respectively. The gain drops are tiny by 0.02 and 0.15 dB, respectively.

The radiation patterns by full-wave simulations are shown in Fig. 10 (a) and (b), respectively, where the cases of uniform excitations are also shown for comparison. Furthermore, in the figures, the angular regions of the TX array to illuminate the RX array and vice versa are also labeled, where low SLLs are achieved in these regions by the proposed technique without sacrificing the gain and sidelobe performances. Indeed, in most areas outside the illuminating angular regions, the patterns remain close to the original cases of uniform excitations. Thus, it indicates that the proposed technique only locally alters the radiation patterns to suppress the mutual coupling interferences.

Figure 11 (a) and (b) further show the near-field equivalent current distributions on the RX antenna array's surface when the TX antenna array is excited by the uniform and optimized excitation weightings to radiate the broadside beam in Fig. 10(a). It is seen that the current strength of the proposed method is at least 30 dB smaller than the case by uniform excitation. This induced current reduction may further avoid the saturation of RX's active RF modules. This behavior is consistent with the trend observed in Fig. 10 (a), except for low current strengths. It is noted that the far-field pattern exhibiting a smaller strength difference in the marked region in Fig. 10(a) is caused by the divergence of EM power propagation. The radiation from the TX antenna array will experience small strengths in the vicinity of the RX array and then propagates, following the divergence theorem, to the far zone. The fields external to the RX array region will also contribute to the nulling areas marked in Fig. 10(a).

VI. CONCLUSION

Mutual coupling between adjacent arrays may significantly interfere with the radiation performance, especially under high-power radiation conditions. The proposed technique optimizes the array excitations to reduce mutual coupling effects between adjacent arrays without substantially distorting the radiation patterns. The effectiveness has been validated by considering directional beam radiations. It has been demonstrated that the reaction power between the two antenna arrays can be reduced by at least 60 dB at the cost of gain drops by less than 0.3 dB from the studies. Even though these low mutual coupling excitations may not be achievable in a real system due to the limits of system sensitivity to the noises and digital T/R devices' discrepancies, the proposed concepts' effectiveness has been validated. Besides, the coupling mechanisms were theoretically analyzed. The technique has been compared to the conventional pattern nulling techniques to show superiority. Future works will incorporate the EM coupling reductions between elements within the same antenna arrays to avoid possibly causing scan blindness [56] when suppressing the inter-array mutual coupling. Both hardware [57] and numerical software techniques shall be examined to enhance the effectiveness.

REFERENCES

[1] M. A. Richards, J. A. Scheer, and W. A. Holm, *Principles of Modern Radar: Basic Principles*. Raleigh, NC, USA: SciTech, 2010.

[2] R. J. Mailloux, *Phased Array Antenna Handbook*, 2nd ed. Boston, MA, USA: Artech House, 2005.

[3] S. Silver, *Microwave Antenna, Theory and Design*, 1st ed. New York, NY, USA: McGraw-Hill, 1949.

[4] W. L. Melvin and J. Scheer, *Principles of Modern Radar: Advanced Techniques*. Raleigh, NC, USA: SciTech, 2013.

[5] L. Qiu, F. Zhao, K. Xiao, S.-L. Chai, and J.-J. Mao, "Transmit–receive isolation improvement of antenna arrays by using EBG structures," *IEEE Antennas Wireless Propag. Lett.*, vol. 11, pp. 93–96, 2012.
[6] S. Ahmed and M. Faulkner, "Optimized interference canceling for colocated base station transceivers," *IEEE Trans. Veh. Technol.*, vol. 60, no. 9, pp. 4175–4183, Nov. 2011.
[7] P. Janpugdee, P. Pathak, R. Burkholder, J. Lee, and X. Wang, "A ray-based sub-aperture approach for the prediction of mutual coupling between conformal arrays on a convex metallic platform," in *Proc. Asia–Pacific Microw. Conf.*, 2009, pp. 1277–1280.
[8] A. C. K. Mak, C. R. Rowell, and R. D. Murch, "Isolation enhancement between two closely packed antennas," *IEEE Trans. Antennas Propag.*, vol. 56, no. 11, pp. 3411–3419, Nov. 2008.
[9] M. Alibakhshikenari, B. S. Virdee, C. H. See, R. Abd-Alhameed, A. H. Ali, F. Falcone, and E. Limiti, "Study on isolation improvement between closely-packed patch antenna arrays based on fractal metamaterial electromagnetic bandgap structures," *IET Microw., Antennas Propag.*, vol. 12, no. 14, pp. 2241–2247, Nov. 2018.
[10] C. Tokgoz, C. J. Reddy, R. J. Burkholder, and P. H. Pathak, "Application of UTD for prediction of radiation pattern and mutual coupling associated with antennas on faceted airborne platforms," in *Proc. IEEE Antennas Propag. Soc. Int. Symp.*, Jun. 2009, pp. 1–4.
[11] Z. Sipus, M. Bosiljevac, and S. Skokic, "Mutual coupling analysis of cylindrical waveguide arrays using hybrid SD-UTD method," in *Proc. IEEE Antennas Propag. Soc. Int. Symp.*, Jul. 2005, pp. 155–158.
[12] P. Pathak and N. Wang, "Ray analysis of mutual coupling between antennas on a convex surface," *IEEE Trans. Antennas Propag.*, vol. AP-29, no. 6, pp. 911–922, Nov. 1981.
[13] H. Miyashita, Y. Sunahara, R. Ishii, T. Katagi, and T. Hashimoto, "An analysis of antenna coupling between arrays on a polyhedron structure," *IEEE Trans. Antennas Propag.*, vol. 41, no. 9, pp. 1242–1248, Sep. 1993.
[14] Q. Xu, M. Biedka, and Y. E. Wang, "Indented antenna arrays for high isolation: The growing interest in simultaneous-transmit-and-receive-based full-duplex communication systems," *IEEE Antennas Propag. Mag.*, vol. 60, no. 1, pp. 72–80, Feb. 2018.
[15] H.-S. Lui, H. T. Hui, and M. Seng Leong, "A note on the mutual-coupling problems in transmitting and receiving antenna arrays," *IEEE Antennas Propag. Mag.*, vol. 51, no. 5, pp. 171–176, Oct. 2009.
[16] M. M. Bait-Suwailam, O. F. Siddiqui, and O. M. Ramahi, "Mutual coupling reduction between microstrip patch antennas using slotted-complementary split-ring resonators," *IEEE Antennas Wireless Propag. Lett.*, vol. 9, pp. 876–878, 2010, doi: 10.1109/LAWP.2010.2074175.
[17] M. S. Sharawi, A. B. Numan, M. U. Khan, and D. N. Aloi, "A dual-element dual-band MIMO antenna system with enhanced isolation for mobile terminals," *IEEE Antennas Wireless Propag. Lett.*, vol. 11, pp. 1006–1009, 2012.
[18] A. K. Bhattacharyya, *Phased Array Antennas: Floquet Analysis, Synthesis, BFNs and Active Array Systems*. Hoboken, NJ, USA: Wiley, 2006.
[19] C. A. Balanis, *Antenna Theory: Analysis and Design*, 4th ed. Hoboken, NJ, USA: Wiley, 2016.
[20] C. L. Dolph, "A current distribution for broadside arrays which optimizes the relationship between beam width and side-lobe level," *Proc. IRE Waves Electrons*, vol. 34, no. 6, pp. 335–348, Jun. 1946.
[21] R. J. Stegen, "Excitation coefficients and beamwidths of Tschebyscheff arrays," *Proc. IRE*, vol. 41, no. 11, pp. 1671–1674, Nov. 1953.
[22] T. T. Taylor, "Design of line-source antennas for narrow beamwidth and low sidelobes," *IRE Trans. Antennas Propag.*, vol. AP-3, no. 1, pp. 16–28, Jan. 1955.
[23] I. Gupta and A. Ksienski, "Effect of mutual coupling on the performance of adaptive arrays," *IEEE Trans. Antennas Propag.*, vol. AP-31, no. 5, pp. 785–791, Sep. 1983.
[24] H. M. Ibrahim, "Null steering by real-weight control—A method of decoupling the weights," *IEEE Trans. Antennas Propag.*, vol. 39, no. 11, pp. 1648–1650, Nov. 1991.
[25] Y. Aslan, J. Puskely, A. Roederer, and A. Yarovoy, "Phase-only control of peak sidelobe level and pattern nulls using iterative phase perturbations," *IEEE Antennas Wireless Propag. Lett.*, vol. 18, no. 10, pp. 2081–2085, Oct. 2019.
[26] T. B. Vu, "On null steering in rectangular planar array," *IEEE Trans. Antennas Propag.*, vol. 40, no. 8, pp. 995–997, Aug. 1992.
[27] J. R. Mohammed, "Element selection for optimized multiwide nulls in almost uniformly excited arrays," *IEEE Antennas Wireless Propag. Lett.*, vol. 17, no. 4, pp. 629–632, Apr. 2018.
[28] K. Yu and M. F. Fernández, "Antenna pattern synthesis with multiple discrete and continuous nulls," in *Proc. IET Intern. Radar Conf.*, 2015, pp. 1–7, doi: 10.1049/cp.2015.1110.
[29] J. R. Mohammed and K. H. Sayidmarie, "Null steering method by controlling two elements," *IET Microw., Antennas Propag.*, vol. 8, no. 15, pp. 1348–1355, Dec. 2014.
[30] M. F. Fernández and K.-B. Yu, "Robust adaptive beamforming with main-lobe maintenance of monopulse beams," in *Proc. IET Int. Radar Conf.*, Nanjing, China, Oct. 2018, pp. 1225–1230.
[31] X. Yang, S. Li, Y. Sun, T. Long, and T. K. Sarkar, "Robust wideband adaptive beamforming with null broadening and constant beamwidth," *IEEE Trans. Antennas Propag.*, vol. 67, no. 8, pp. 5380–5389, Aug. 2019.
[32] M. H. Er, "Linear antenna array pattern synthesis with prescribed broad nulls," *IEEE Trans. Antennas Propag.*, vol. 38, no. 9, pp. 1496–1498, Sep. 1990.
[33] S. Prasad, "Linear antenna arrays with broad nulls with applications to adaptive arrays," *IEEE Trans. Antennas Propag.*, vol. AP-27, no. 2, pp. 185–190, Mar. 1979.
[34] L. D. Nguyen, H. D. Tuan, T. Q. Duong, and H. V. Poor, "Multi-user regularized zero-forcing beamforming," *IEEE Trans. Signal Process.*, vol. 67, no. 11, pp. 2839–2853, Jun. 2019.
[35] Z. Wang and W. Chen, "Regularized zero-forcing for multiantenna broadcast channels with user selection," *IEEE Wireless Commun. Lett.*, vol. 1, no. 2, pp. 129–132, Apr. 2012.
[36] R. Vescovo, "Power pattern synthesis for antenna arrays with null constraints in the near-field region," *Microw. Opt. Technol. Lett.*, vol. 44, no. 6, pp. 542–545, Mar. 2005.
[37] A. H. Mohammadian, S. S. Soliman, M. Ali Tassoudji, and L. Golovanevsky, "A closed-form method for predicting mutual coupling between base-station dipole arrays," *IEEE Trans. Veh. Technol.*, vol. 56, no. 3, pp. 1088–1099, May 2007.
[38] V. H. Rumsey, "Reaction concept in electromagnetic theory," *Phys. Rev.*, vol. 94, no. 6, pp. 1483–1491, Jun. 1954.
[39] H.-T. Chou, "Maximization of mutual reaction between two conformal phased arrays of antennas to enhance power transfer in radiating near-field region," *IEEE J. Radio Freq. Identificat.*, vol. 4, no. 4, pp. 506–516, Dec. 2020.
[40] M. F. Fernández and K.-B. Yu, "Blocking-matrix and quasimatrix techniques for extended-null insertion in antenna pattern synthesis," in *Proc. IEEE Radar Conf. (RadarCon)*, May 2015, pp. 198–203.
[41] G. Golub and C. Van Loan, *Matrix Computations*, 3rd ed. Baltimore, MD, USA: John Hopkins University Press, 1996.
[42] B. D. Van Veen, "Eigenstructure based partially adaptive array design," *IEEE Trans. Antennas Propag.*, vol. 36, no. 3, pp. 357–362, Mar. 1988.
[43] W. Geyi, *Foundations of Applied Electrodynamics*. Chichester, U.K.: Wiley, May 2010, pp. 273–275.
[44] H.-T. Chou, "Equivalent orthogonal beam steering for fast determination of reactions between two phased arrays of antennas with analog beamforming networks for maximum wireless power transfer," *IEEE Trans. Antennas Propag.*, vol. 69, no. 12, pp. 8449–8460, Dec. 2021, doi: 10.1109/TAP.2021.3090517.
[45] T. S. Bird, *Mutual Coupling Between Antennas*. New York, NY, USA: Wiley, 2021.
[46] J. Lundgren, J. Malmström, J. -M. Hannula, and B. L. G. Jonsson, "Visualization and reduction of mutual coupling between antennas installed on a platform," *IEEE Trans. Electromagn. Compat.*, vol. 64, no. 1, pp. 92–101, Feb. 2022.
[47] J. Malmström, H. Holter, and B. L. G. Jonsson, "On mutual coupling and coupling paths between antennas using the reaction theorem," *IEEE Trans. Electromagn. Compat.*, vol. 60, no. 6, pp. 2037–2040, Dec. 2018.
[48] W. L. Stutzman and G. A. Thiele, *Antenna Theory and Design*, 2nd ed. New York, NY, USA: Wiley, 1998.
[49] Y. Urzhumov and D. R. Smith, "Metamaterial-enhanced coupling between magnetic dipoles for efficient wireless power transfer," *Phys. Rev. B, Condens. Matter*, vol. 83, no. 20, May 2011, Art. no. 205114.
[50] K.-C. Lee and T.-H. Chu, "A circuit model for mutual coupling analysis of a finite antenna array," *IEEE Trans. Electromagn. Compat.*, vol. 38, no. 3, pp. 483–489, Aug. 1996.
[51] B. A. Munk, *Finite Antenna Arrays and FSS*. Hoboken, NJ, USA: Wiley, 2003.
[52] D. F. Kelley, "Relationships between active element patterns and mutual impedance matrices in phased array antennas," in *Proc. IEEE Antennas Propag. Soc. Int. Symp.*, Jun. 2002, pp. 524–527.

[53] H. Bui-Van, V. Hamaide, C. Craeye, F. Glineur, and E. D. L. Acedo, "Direct deterministic nulling techniques for large random arrays including mutual coupling," *IEEE Trans. Antennas Propag.*, vol. 66, no. 11, pp. 5869–5878, Nov. 2018.
[54] D. K. Cheng, *Field, and Wave Electromagnetics*. Reading, MA, USA: Addison-Wesley, 1989.
[55] *Ansys HFSS*, Ansys, Canonsburg, PA, USA, 2021.
[56] D. Pozar and D. Schaubert, "Scan blindness in infinite phased arrays of printed dipoles," *IEEE Trans. Antennas Propag.*, vol. AP-32, no. 6, pp. 602–610, Jun. 1984, doi: 10.1109/TAP.1984.1143375.
[57] M. A. Khayat, J. T. Williams, D. R. Jackson, and S. A. Long, "Mutual coupling between reduced surface-wave microstrip antennas," *IEEE Trans. Antennas Propag.*, vol. 48, no. 10, pp. 1581–1593, Oct. 2000, doi: 10.1109/8.899675.

HSI-TSENG CHOU (Fellow, IEEE) received the B.S. degree in electrical engineering from National Taiwan University, Taiwan, in 1988, and the M.S. and Ph.D. degrees in electrical engineering from The Ohio State University (OSU), in 1993 and 1996, respectively.

He is currently a Distinguished Professor with the Graduate Institute of Communication Engineering and the Department of Electrical Engineering, National Taiwan University. He joined the ElectroScience Laboratory (ESL), OSU, as a Graduate Research Associate, from 1991 to 1996, and a Postdoctoral Researcher, from 1996 to 1998. His research interests include wireless communication networks, antenna design, antenna measurement, electromagnetic scattering, asymptotic high-frequency techniques, such as the uniform geometrical theory of diffraction (UTD), novel Gaussian beam techniques, and UTD type solution for periodic structures. He has published more than 493 journals and conference papers, and holds 40 patents.

Dr. Chou has received many awards to recognize his distinguished contributions to technological developments. Some important ones include the Distinguished Contribution Award in promoting inter-academic and industrial cooperation from the Ministry of Education, the Distinguished Engineering Professor Award from the Chinese Institute of Engineers, the Distinguished Electrical Engineering Professor Award from the Chinese Institute of Electrical Engineering, the University's Industrial Economics Contribution Award, in 2008, the National Industrial Innovation Awards—Key Technology Elite Award, in 2011, and the Industrial-Academia Collaboration Award, in 2017, all from Ministry of Economics. He was elected as one of the nation's ten outstanding young persons by Junior Chamber International, in 2004, a National Young Person Medal from China Youth Corps of Taiwan, in 2005, and one of the top ten rising stars in Taiwan by the Central News Agency of Taiwan. He has served as the Chair for the IEEE AP-S Taipei Chapter. He received the Best Chapter Award, in 2012. He is the former Chair of the EMC-S Taipei Chapter. He also received outstanding branch counselor awards from IEEE, including IEEE headquarter, R-10 and Taipei Section. He received the IEEE Technical Field Undergraduate Teaching Award, in 2014. He is an IET Fellow and an elected member of URSI International Radio Science U.S. Commission B.

CHEN-YI CHANG (Graduate Student Member, IEEE) received the B.S. degree in electronic and communication engineering from the City University of Hong Kong, Hong Kong, in 2015. He is currently pursuing the Ph.D. degree in communication engineering with the Graduate Institute of Communication Engineering, National Taiwan University, Taipei, Taiwan. His current research interests include high-gain antenna design and beamforming techniques for 5G mobile communication.

DANAI TORRUNGRUENG (Senior Member, IEEE) received the B.Eng. degree in electrical engineering (EE) from Chulalongkorn University, Bangkok, Thailand, in 1993, and the M.S. and Ph.D. degrees in EE from The Ohio State University (OSU), in 1996 and 2000, respectively.

From 1995 to 2000, he was a Graduate Research Assistant (GRA) with the Department of Electrical Engineering, ElectroScience Laboratory, OSU. From 2002 to 2017, he was with the Electrical and Electronic Engineering Department, Faculty of Engineering and Technology, Asian University, Chonburi, Thailand. He is currently a Professor with the Department of Teacher Training in Electrical Engineering, Faculty of Technical Education, King Mongkut's University of Technology North Bangkok, Bangkok, Thailand. In 2000, he won an award in the National URSI Student Paper competition at the 2000 National Radio Science Meeting in Boulder, CO, USA. From 2004 to 2009, he invented generalized Smith charts, called T-charts or Meta-Smith charts, to solve several problems associated with conjugately characteristic-impedance transmission lines (CCITLs) and bi-characteristic-impedance transmission lines (BCITLs), including their useful applications in applied electromagnetics. He has authored *Meta-Smith Charts and Their Potential Applications* (Morgan and Claypool, 2010) and *Advanced Transmission-Line Modeling in Electromagnetics* (Charansanitwong Printing, 2012). His research interests include electromagnetic sensors, fast computational electromagnetics, rough surface scattering, propagation modeling, electromagnetic wave theory, microwave theory, and techniques and antennas. He is currently a member of the ECTI, where he served as an ECTI Technical Chair of Electromagnetics, from 2014 to 2017. In addition, he served as the TPC Co-Chair for TJMW2016, the Vice Co-Chair for TJMW2017, and the TPC Chair for ISAP2017. Furthermore, he is the Co-Founder of the Innovative Electromagnetics Academy of Thailand (iEMAT), in 2013.